A Novel Active Pixel Sensor With On-Pixel Analog-to-Digital Converter for Mammography

C. D. Arvanitis, S. E. Bohndiek, G. Segneri, C. Venanzi, G. Royle, A. Clark, J. Crooks, R. Halsall, M. Key-Charriere, S. Martin, M. Prydderch, R. Turchetta and R. Speller

Abstract–Two acitve pixel sensor (APS) architectures have been evaluated for mammography. Firstly, a 525 x 525 APS array of 25 x 25 µm pixels with greater than 80% fill factor, on-pixel analogue buffer amplifier and column parallel 10-bit ADC has been optically coupled to a 115 µm thick CsI:Tl phosphor with columnar structure. Critical performance parameters such as photon transfer curves, MTF, and DQE have been measured. With a readout rate of 10 f/sec, the sensor has a read noise of 114 ± 2 e- and suffers from read related column FPN. A DQE of 35 % close to zero frequency has been measured for this array. Secondly, a novel APS test structure with on-pixel ADC, i.e. On Pixel Intelligent CMOS (OPIC), has been designed to eliminate the above limitations. This sensor, a 72 x 64 array, is almost free of column FPN, reads at rates more than 3700 f/sec and exhibits 44±5 e- read noise. Additionally, a "hit flag" can be set to select only pixels above a threshold for sparse readout. By adjusting the threshold, segmentation of different regions of the image can be performed. The time above threshold can also be recorded, offering a technique to eliminate over-exposed mammograms. Both sensors had 10 % MTF at 9 cycles/mm when coated with the structured CsI:Tl. X-ray images displaying the sensors capabilities are also presented.

I. Introduction

CMOS sensors with on-pixel analogue buffer amplifier [1], low read related noise [2], and fast image acquisition through massive parallel read out are being developed for scientific applications. As technology downscales both increased sensitivity in the blue part of the spectrum [3] and higher fill factor [4] are expected. Large area CMOS monolithic active pixel sensors (APS) with zero dead area can be produced due to advances in stitched technology, making these a viable alternative to flat panel imagers.

Planar and advanced digital mammography [5] could benefit from the on-pixel characteristics of CMOS APS. Low noise, high fill factor and good spectral matching with CsI:Tl phosphors will improve the "image quality" in digital mammography. In contrast enhanced mammography higher signal-to-noise ratio at regions with lower contrast medium concentration of the breast could be achieved. Fast image acquisition is essential for tomosynthesis and mammotomography to minimize patient motion artifacts.

Manuscript received November 13, 2006. This work is supported by the RC-UK Basic Technology Multidimensional Integrated Intelligent Imaging (MI-3) programme (GR/S85733/01).

C. Arvanitis, S. Bohndiek, G. Segner, C. Venanzi, G. Royle and. R. Speller are with the department of Medical Physics and Bioengineering at University College London, London, UK
(e-mail: akostas@medphys.ucl.ac.uk).

A. Clark, J. Crooks, R. Halsall, M. Key-Charriere, S. Martin, M. Prydderch and R. Turchetta are with the Rutherford Appleton Laboratories Chilton, Didcot, Oxfordshire, OX11 0QX, UK

II. Methods and Materials

Two monolithic APS have been employed in this study; a standard 3T APS (Fig. 1. a) and a novel APS that offers high pixel level integration (Fig. 1. b) utilizing the recent advances in standard CMOS technology. Description of the two pixel architectures is given below. The performance of the two sensors in terms of read noise, full well capacity and signal-to-noise ratio has been evaluated optically through the photon transfer curve (PTC) technique. The two sensors were optically coupled via a fiber optic plate to structured CsI:Tl phosphors, and their x-ray imaging performance has been evaluated by measuring their energy dependent modulation transfer function (MTF), noise power spectrum (NPS) and detection quantum efficiency (DQE).

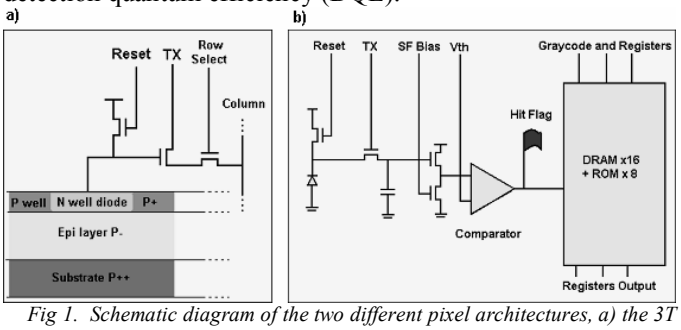

Fig 1. Schematic diagram of the two different pixel architectures, a) the 3T APS with the nwell photodiode, the reset, the source follower (TX), and the column select transistor b) the OPIC with the read out transistors, on-pixel ADC, comparator, and "hit flag".

A. APS Pixels

The 3T APS is a 525 x 525 array based on almost 100% fill factor technology with 25 x 25 µm pixel pitch and on-chip column parallel 10-bit analog-to-digital converters (ADC) that reads at 10 frames/sec [6]. Each pixel has 4 n-well photodiodes (PD) as sensing elements, reset, source follower (TX), and row select transistors (Fig. 1. a) offering the highest possible fill factor.

The novel APS test structure with on-pixel ADC will be referred to in this paper as On Pixel Intelligent CMOS (OPIC). It allows high-speed read-out (>3700 frames/sec) and snap shot digital imaging. This structure comprises a 72 x 64 pixel array with 30 x 30 µm pixel pitch. Each pixel has an n-well

photodiode, source follower (TX), reset transistor, storage capacitor, two in-pixel DRAM 8-bit memories and a comparator (Fig. 1. b). The OPIC sensor with on-pixel ADC enables high frame rate and offers increased on-pixel functionality. Three different read out modes are possible. The first is the raw ADC value corresponding to the pixel signal. The second is the address of pixel location for sparsification of the image. The third is a time related value that records the time taken for the pixel signal to cross an external threshold. The on-pixel comparator compares the pixel signal level to the global threshold value and a "hit flag" is set to select only pixels above the threshold for sparse readout. The two in-pixel DRAM memories are used to store an 8-bit gray coded value equivalent to ADC value following voltage conversion, and also the time-related code when the diode passes the global threshold voltage. In Table I the design specifications of the two sensors are given. In both sensors the voltage (Vdd) applied to the reset transistor was 3.3 Volts. In Fig. 2 the OPIC sensor board and the FPGA-based data acquisition (DAQ) hardware of the sensors is displayed. Embedded functions on the FPGA-based DAQ of the sensors can enhance the on-chip capabilities.

The 3T APS was developed for charge particle tracking and named as "Startracker" [6]. However, as the sensor can be used for visible light detection, it can be optically coupled to phosphors for indirect x-ray detection.

TABLE I

	3T APS	OPIC
Pixel format	525 x 525	72 x 64
Pixel pitch	25 um	30 um
Array dimension	13 x13 mm^2	2 x 2 mm^2
Optical fill factor	>80%	~ 10 %
Process	0.5 um CMOS	0.35 um CMOS
Optical sensor	NWell photodiode	NWell photodiode
Frame rate	10 fps	>3700 fps
ADC	10 bits (column parallel)	8 bits (per pixel)

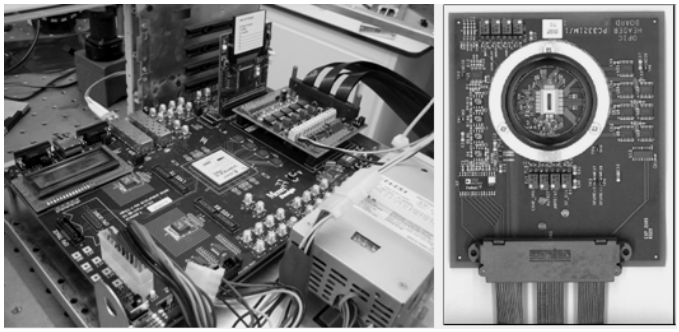

Fig 2. The FPGA-based DAQ of the sensors and the OPIC sensor board.

B. Photon Transfer

The photon transfer curve is used to characterize and optimize CCD and CMOS sensors in absolute units [7]. The relative digital signal generated by the on-chip ADC, expressed in raw digital numbers (DN) is converted to absolute electron units through the camera gain constant,

$$K\left(e^{-}/DN\right)=\frac{S(DN)}{N_{SN}(DN)^2} \qquad (1)$$

where N_{SN} is the signal shot noise.

The PTC data in Fig. 3 generated by varying the light intensity incident upon a uniformly irradiated region of 100 x 100 pixels on the APS, from dark until saturation. The r.m.s. noise as a function of pixel signal is plotted logarithmically in the PTC. The three noise curves presented are A) all noise components that incorporate read, shot, and fixed pattern noise, B) read and shot noise and C) shot noise. The third curve is used to optimize the sensor by achieving shot noise limited performance (slope of ½, i.e. the noise changes by the square root of the signal). Three regions can be identified in the curve that has all noise components. The first region has zero slope and is dominated by read noise, the second with slope ½ is dominated by shot noise from both the signal and sensor electronics. At higher signal levels, the slope is ~1 where the fixed pattern noise is the dominant noise component of the signal.

The read noise and full well capacity are converted from relative digital numbers to absolute units of electrons after measuring the camera gain constant (e^{-}/DN). Signal-to-noise ratio (SNR) and dynamic range (DR) can be measured using the signal and the r.m.s. noise from the shot noise limited curve.

C. X-ray Characterization

The 3T APS was optically coupled via 5 mm thick fiber optic plate to 115 μm thick structured CsI:Tl (referred to as CsI in the remainder of the paper). A 100 μm thick CsI layer was optically coupled to the OPIC sensor through a 1 mm thick fiber optic plate. Their energy dependent modulation transfer function (MTF) was measured.

A prototype micro focus X-ray tube (X-Tek systems Ltd) with Mo/Mo target/filter combination, operated at 30 kVp was used for the measurements. The presampling MTF was estimated using a 10 μm (± 1 μm) slit camera. The angle of the slit with respect to the detector pixel matrix was ~2^0. The magnification of the slit was less than 1 %. The slit images were offset and gain variations corrected. Additionally, 7 MTFs were averaged to improve accuracy.

For the NPS measurements the beam was hardened by 4 cm of polymethyl methacrylate (PMMA) and the two dimensional noise power spectrum (NPS) of a 128x128 central region of the image was measured. 50 realizations were sufficient to achieve a smooth NPS. Offset and background trends such as heel effect, were removed by means of dark and ROI surface fitted subtraction. For the 1D NPS data, a thick slice directly adjacent to the frequency axis, comprising eight lines on either side of the axis (excluding the axis) was taken from the 2D NPS, in order to further smooth the spectrum.

The exposure was measured with a calibrated ionization chamber (KEITHLEY 35050A Dosimeter) placed between the 4 cm PMMA and the sensor. From the x-ray spectral distribution, the exposure and the x-ray photon flux per unit

area was measured. The detection quantum efficiency (DQE) was measured according to the empirical equation

$$DQE(f) = \frac{MTF^2(f)}{NPS_{Normalized}(f)q} \qquad (2)$$

where q is the x-ray photon flux per unit area.

D. X-Ray imaging with On - Pixel Intelligent CMOS

The three different outputs described in Section II.A. were tested under x-ray conditions. The on-pixel capabilities are demonstrated by imaging a small tube filled with contrast medium. The tube had internal diameter of 1 mm and external diameter of 2 mm and placed directly in front of the sensor. The images were acquired, using Tungsten (W) X-ray tube at 50 kVp load and 15 mA current. The different images are presented in Fig. 9.

III. Results

A. Optical Performance Evaluation

The PTC of the 3T APS is displayed in Fig. 3. Shot noise limited performance was achieved as can be seen from slope of ½, indicating optimum operating conditions. Corrections for nonlinearity response of the sensors have been performed [7]. The error bars in the PTC plot are smaller than the points (1.6%). Similar curve was measured for the OPIC, although the performance in this case is not shot noise limited. In Table II the performance parameters extracted from the photon transfer curve of the two sensors are given.

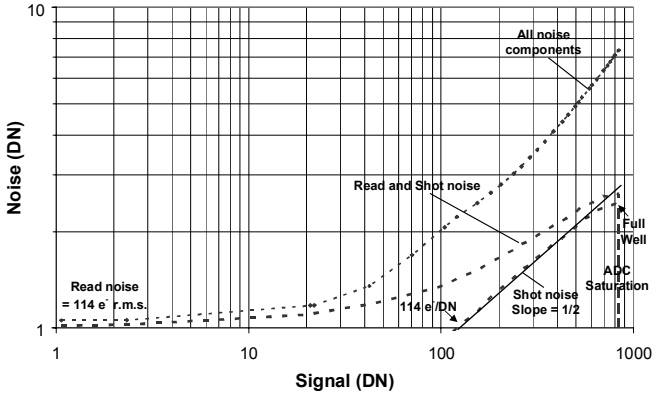

Fig. 3. The photon transfer curve of the 3T APS.

TABLE II

Performance Parameters	3T APS	OPIC	Units
Camera Gain	114 ± 2	25 ± 4	electrons/DN
Read Noise	114 ± 2	44 ± 5	electrons
Full Well	10^5	$8x10^4$	electrons
Integral Non-linearity (max)	3.7	16	%
Shot noise limited SNR	50	52	dB
Dynamic Range	59	65	dB

The 3T APS has high read noise of 114 e^- but good signal-to-noise ratio (SNR) and dynamic range (DR). The OPIC APS has read noise of 50 e^-, and better SNR and DR than the 3-T APS. This sensor is almost free of read related column FPN as can be seen from its dark image (Fig. 4 b). On the contrary the 3T APS has high read related column FPN (Fig. 4. a).

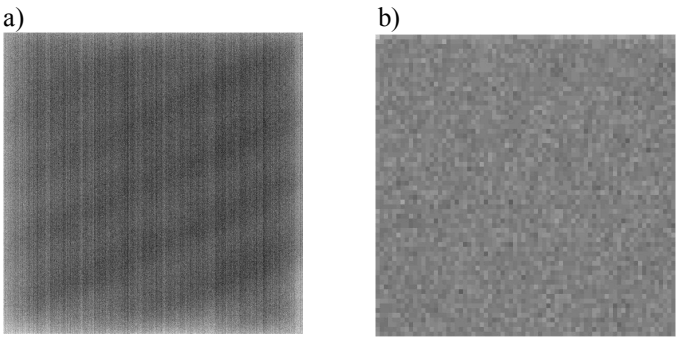

Fig 4. Dark images of the two sensors displaying the read related column FPN. a) The 3T APS, and b) the OPIC. The image of the OPIC sensor has been magnified for visualization purposes.

B. X-Ray Performance Evaluation

Once the sensors have been characterized and optimized through the PTC they were coupled via fiber optic plate to CsI. The MTF of the OPIC and the 3T APS are displayed in Fig 5.

The row NPS of the 3T APS both with and without x-ray irradiation is displayed in Fig 6. Note that y-axis in the raw NPS is expressed in absolute units since the digital pixel signal has been converted to electrons through the camera gain constant.

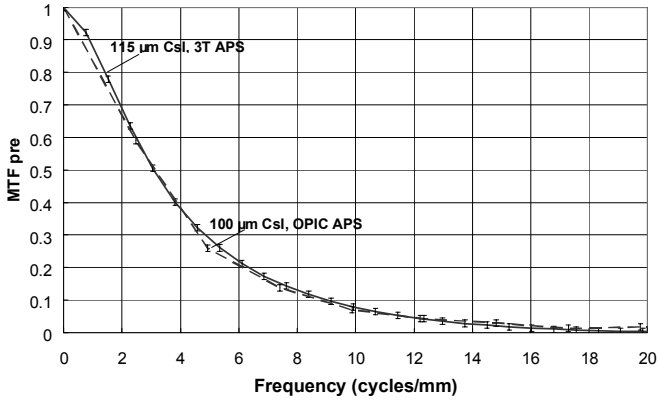

Fig. 5. The MTF of the OPIC coupled to 100 micron CsI (dashed line), and the 3T coupled to 115 micron CsI (solid line).

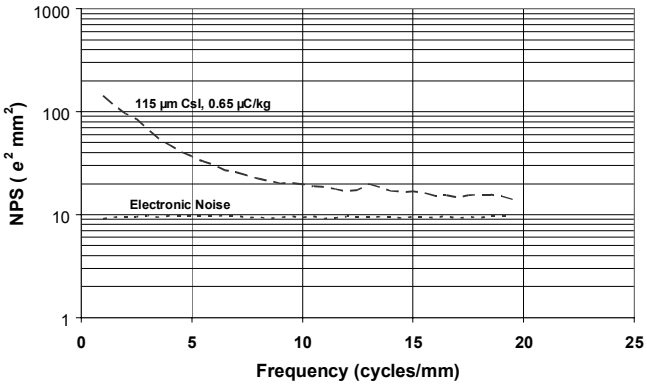

Fig 6. Row NPS of the 3T APS electronic noise and the x-ray detector.

In Fig. 7 the DQE of the 3T APS is displayed. The DQE close to zero frequency of the 3T APS was 35% at detector entrance exposure of 0.65 μC/kg. The measurement of the NPS and DQE of the OPIC due to its small physical size and low fill factor was not possible to perform.

To further evaluate the potential of the 3T APS for mammography an image of a 1 cm thick breast tissue sample superimposed on 3 cm PMMA was acquired under typical mammographic exposure. The total entrance exposure was 282.5 μC/kg. The breast sample incorporates breast tumor (upper left corner of Fig. 8) and fatty tissue (bottom right corner of Fig. 8) as marked by an expert radiologist.

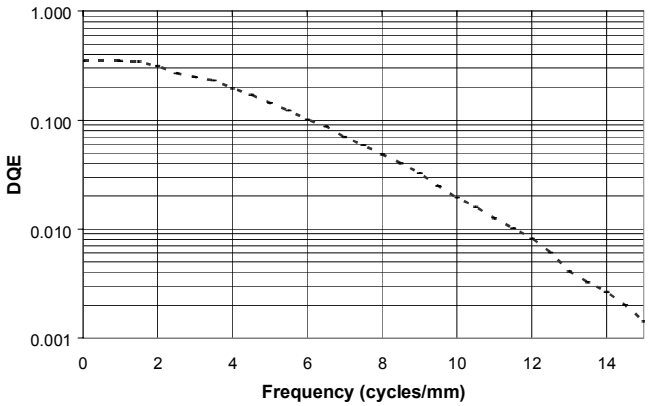

Fig 7. DQE of the 3T APS optically coupled to CsI.

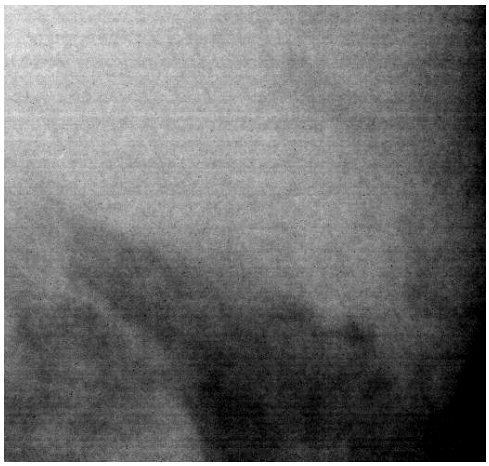

Fig. 8. X-ray image of a 1 cm thick breast tissue superimposed to 3 cm PMMA 4 cm. The image intensity has been reversed.

C. On Pixel X-ray Intelligent CMOS imaging

In Fig. 9 the different modes of operation of the OPIC are displayed with the aid of a small tube filled with contrast medium. In Fig. 9 a) and b), the raw digital image under unsaturated and partially saturated conditions is shown. The sparse readout and timing image are shown in Fig. 9 c) and d) respectively. The dark part of the raw digital image displays the 2 mm thick tube. The sparse image is a binary image having "1" when the threshold reached and "0" otherwise. The time related image was acquired when the digital image was saturated in order to fully display the on-pixel capabilities of this sensor. All three images can be read from the pixel. The vertical line features seen in the images are data from "repeater pixels" that include clock buffers and additional logic to ensure data integrity so the hit flag is always set to "1". Due to scintillator edge effects the first 9 columns of the sensor had very low gain and thus excluded from the images.

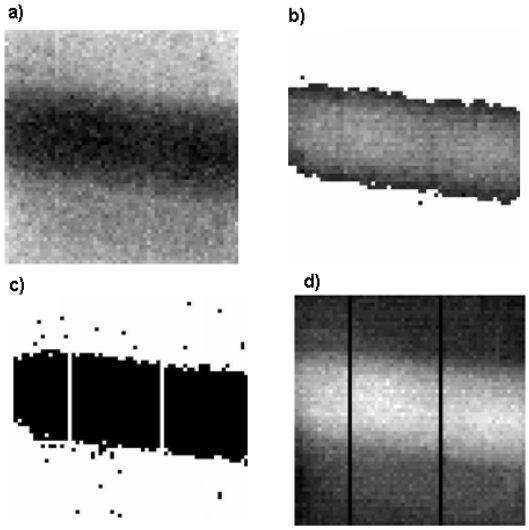

Fig 9. Images of the three different on-pixel registers of the OPIC, a) digital image,b)saturated digital image c) sparse image, and d) time image. The images are magnified for visualization purposes. A W tube with 50 kVp load, 15 mA, integration time 32 msec and 164 msec for the images a) and b) respectively was used.

IV. Discussion

In CMOS APS under development, performance optimization can be achieved through PTC analysis. Shot noise limited performance is needed for optimum operation of a detector and evaluation for medical imaging. Critical performance parameters (Table II) can be measured in absolute units offering unique inside to the detector performance.

The 3T APS offers very high fill factor and provides a reliable CMOS APS sensor that can be used as reference in order to compare any new sensor designs developed to offer improved performance. High full well capacity, SNR and DR are some of the critical performance parameters essential for medical imaging. This sensor is limited by the reset kTC noise. The kTC noise originates from the photodiode parasitic capacitance when the sense node (TX) is reset.

The OPIC offers better noise performance due to its smaller capacitance. The SNR and DR of the OPIC are better as a result of its improved noise performance. APS sensors exhibit column related read noise (Fig 4. a). In the 3T APS this noise arises from small fluctuations in column amplifiers. The OPIC APS is free of this type of noise due to the absence of column amplifiers. At high pixel value levels an offset fixed pattern noise (FPN) appears between odd and even lines due to the pixel design used to improve fill factor.

The high full well capacity (~10^5 e^-) of the sensors is primarily determined by their pixel size once more photocharge can be collected. As the pixel size decreases better noise performance is achieved at the cost of dynamic range. This trade off becomes less apparent if off pixel or on pixel methods are employed to eliminate kTC noise [2].

Performance evaluation of x-ray imagers is performed in the frequency domain by measuring objective criteria such as MTF, NPS, and DQE.

The MTF of both systems is similar and is primarily determined by the CsI phosphor [8]. The physical size of the sensors prevented us from using the same CsI phosphor. The differences of the MTFs are within the experimental error indicating that the small phosphor thickness difference did not change the resolution of the systems. This is the case as the columnar structure of CsI acts as an optical guide for the scintillating photons preventing lateral spreading. Both systems had 10% MTF at 9 cycles/mm indicating that these phosphors have been optimized for high resolution and are suitable for mammography.

Further x-ray evaluation of the OPIC sensor was not possible for two reasons. First, its physical size was only 72 x 64 that limited the region of the image for the NPS estimation to 32 x 32 pixels. Second, the high level of on-pixel integration of the OPIC sensor resulted in a fill factor of around 10%, much lower than the 3T APS. This is not an inherent limitation of the pixel architecture once higher pixel sizes can be employed to increase the fill factor and sensitivity.

The 1D NPS of the 3T APS (Fig. 6) shows that at middle to low frequencies the electronic noise was substantially lower than the total system noise that includes the x-ray component. At frequencies above 10 cycles/mm was equal to the half of total noise. This indicates that at low exposures (0.65 μmC/kg) high frequency electronic noise might affect the performance of the system.

The DQE of the system was measured according to empirical equation (2). DQE of 35% close to zero frequency sets the upper limit of detection efficiency of the system. The DQE at 0.65 μmC/kg detector entrance exposure is limited above 10 cycles/mm indicating that small anatomic structures can be effectively visualized. This is a very good performance for a sensor developed under standard CMOS process [8].

The image of the breast tissue taken under typical mammographic conditions with this detector demonstrates encouraging results for visualization of breast tumors when employing CMOS APS technology.

Based on the above experimental analysis we anticipate that APS sensors can provide even better performance for medical imaging. Use of a smaller CMOS process (<0.25 μm) and a foundry specialized for CMOS image sensors (CIS process) will improve the performance of new sensors.

The on-pixel capabilities of the OPIC sensor have been presented (Fig. 9) by imaging of a tube filled with iodinated contrast medium. The iodinated contrast medium tube was selected in order to asses the pixel functionality for contrast enhanced imaging. The energy spectrum was selected in order to have reasonably high energy component above the iodine K-edge. By adjusting the global threshold of the sensor, segmentation of the image can be performed in order to directly extract local information of the underlying tissue. We anticipate that sparse read out in regions of increased contrast uptake might provide an alternative and dose effective method to obtain contrast enhanced images. Careful calibration of the system will be necessary. Additionally, by setting the threshold just before saturation overexposed images can be preserved by storing the time taken to reach saturation.

We feel that different medical imaging applications can benefit from the unique characteristics of the OPIC sensor. In this brief our aim was to demonstrate the on pixel capabilities of the sensor. This sensor is a test structure that was fabricated to provide proof of pixel level intelligent medical imaging. The proof of principle provided opens new possibilities and numerous potential benefits when APS technology is used for medical imaging.

V. CONCLUSION

A novel APS i.e. On Pixel Intelligent CMOS (OPIC), and a standard 3T APS have been employed and evaluated for digital mammography. Critical performance parameters of the two active pixel sensors have been measured. Optimization of their performance has been achieved through the photon transfer curve. Improvements in the sensor read noise and column related read noise have been demonstrated when choosing different pixel architecture. The improved noise performance comes at the cost of lower fill factor. High resolution performance from both sensors has been achieved when optically coupled to CsI phosphors (MTF(9)=10%). The 3T APS offers 35% DQE close to zero frequency a very good performance for a sensor developed under standard CMOS process. The image of the breast phantom taken under typical mammographic conditions demonstrates encouraging results for visualization of breast cancer. True on-pixel intelligent imaging has been presented using the novel OPIC sensor.

ACKNOWLEDGMENT

C. Arvanitis is funded by the Greek State Scholarships Foundation. We would like to thank NERC to allow the MI3 consortium to re-manufacture the StarTracker sensor. This sensor was originally designed and first manufactured under NERC funding. We would like to thank Applied Scintillation Technologies (AST) for providing the phosphor samples. Many thanks go to Dr A. Olivo for many discussions and useful comments throughout the conduction of this work.

REFERENCES

[1] E. R. Fossum “CMOS Image Sensors: Electronic Camera-On-A-Chip” IEEE. Trans. Electron Devices, vol. 44, pp. 1689-1698, 1997.

[2] H. Tian, B. Fowler, and A. El Gamal “Analysis of Temporal Noise in CMOS Photodiode Active Pixel Sensor” IEEE Solid-State Circ., Vol. 36, pp. 92-101, 2001.

[3] T. Lulé et. al. “Sensitivity of CMOS Based Imagers and Scaling Perspectives” IEEE. Trans. Electron Devices, vol. 47, pp. 2110-2122, 2000.

[4] H. Wong “Technology and Device Scaling Considerations for CMOS Imagers” IEEE. Trans. Electron Devices, vol. 47, pp. 2110-2122, 2000.

[5] E. D. Pissano, M. J. Yaffe “State of the art: Digital Mammography” Radiol. Vol. 234, pp 353-362, 2005.

[6] R. Turchetta et. al. “A monolithic active pixel sensor for charged particle tracking and imaging using standard VLSI CMOS technology,” Nucl. Instrum. Meth., vol. A 458, pp. 677–689, 2001.

[7] J. Janesick “Lux transfer: Complementary metal oxide semiconductors versus charge-coupled devices” Opt. Eng., Vol. 41, pp. 1203-1215, 2002.

[8] W. Zhao, G. Ristic, and J. A. Rowlands “X-ray imaging performance of structured cesium iodide scintillators” Med. Phys. Vol. 31, pp. 2594-2605, 2004.